Original Paper

Eletrônica de Potência
Open Journal of Power Electronics

Received July 19, 2024; accepted January 16, 2025; Date of publication February 20, 2025.
The review of this paper was arranged by Associate Editor Montiê A. Vitorino and Editor-in-Chief Heverton A. Pereira.

Digital Object Identifier http://doi.org/10.18618/REP.e202522

An Isolated Active-Clamped Circuit Current-Fed Half-Bridge Converter

Glauco E. R da Silva. [1,*], Carlos M. de O. Stein[1], Jean P. da Costa[1], Emerson G. Carati[1], Rafael Cardoso[1], Gustavo W. Denardin[1], Jhon B. B. Quispe[2]

[1]Federal University of Technology – Paraná, Department of Electrical Engineering, Pato Branco, PR, Brazil.
[2]Santa Catarina State University - Electric Power Processing Group - nPEE, Joinville – SC, Brazil.

e-mail: glauco@utfpr.edu.br*; cmstein@utfpr.edu.br; jpcosta@utfpr.edu.br; emerson@utfpr.edu.br; rcardoso@utfpr.edu.br; gustavo@utfpr.edu.br; jhon.quispe@udesc.br.
*Corresponding author

ABSTRACT This paper presents an isolated regenerative active-clamped circuit designed for the current-fed half-bridge (IRACCFHB) converter. Its primary function is to reduce high voltage spikes across the main switches caused by energy stored in the leakage inductance of the power transformer using a clamping capacitor. This recovered energy is delivered efficiently to the load, maintaining the converter's high efficiency and voltage ratio. The proposed auxiliary circuit employs a single active switch with the same ground reference as the main switches, eliminating the need for an isolated gate driver. The converter achieves zero voltage switching (ZVS) during the turn-off of the main switches and zero current switching (ZCS) during the turn-on of the auxiliary switch. Energy recovery to the load is accomplished without compromising galvanic isolation due to employing a coupled inductor in the auxiliary circuit. To validate the proposed analysis and design, a 350 W prototype was implemented.

KEYWORDS Current-fed half-bridge, isolated regenerative active-clamped circuit, zero current switching, zero voltage switching.

I. INTRODUCTION

Current-fed and voltage-fed converters are common isolated topologies used in renewable energy systems. Current-fed converters, in particular, offer advantages such as smaller input current ripple and a higher transformer utilization factor, making them well-suited for microinverter applications [1], [2]. Among current-fed topologies, the current-fed half-bridge (CFHB) uses fewer active switches than the current-fed full-bridge (CFFB), resulting in lower cost and simpler construction. However, CFHBs encounter challenges such as high voltage spikes and ringing across switches during turn-off caused by the transformer's leakage inductance. These issues require the use of switches with a high breakdown voltage, which can potentially reduce converter efficiency due to the proportional increase in on-resistance with drain-source voltage.

The literature contains analyses of soft-switching operation, voltage stress on switches, and topological variations considering the converter in resonant operation. In applications such as PV, fuel cells, battery banks, and others, the current drawn from the power source should exhibit low ripple. This parameter is crucial for the proper functioning of the generation system, as it maximizes energy production and extends the lifespan of these systems, while also helping the converter comply with electromagnetic interference (EMI) regulations [3].

To mitigate issues in isolated converters, passive snubbers, and active clamps are employed to manage energy stored in leakage inductance. Passive snubbers are simpler and less expensive but dissipate energy, thereby reducing converter efficiency. In contrast, active clamps can recover energy, improving efficiency by enabling soft-switching. This approach minimizes switching losses and overvoltages, facilitating the use of higher switching frequencies that contribute to reducing the size of the converter [4], [5].

Active-clamped circuits have been proposed for the CFHB converter. One such design, detailed in [6], is the active-clamped CFHB (ACCFHB) with a full-wave rectifier. This configuration utilizes two switches and a capacitor to clamp the voltage across the main switches, achieving zero-voltage switching (ZVS) for all switches during turn-on. However, it requires two additional drivers, which can increase both cost and volume. Further analysis of the ACCFHB under varying load and input voltages is discussed in [7] and [8]. Another variation of the ACCFHB involves an auxiliary circuit where clamping capacitor shares the ground with main switches, as presented in [9].

Additionally, [10] presents an active-clamped zero-current switching (ZCS) CFHB converter comprising a single switch, capacitor, and inductor, as illustrated in Fig. 1. This design absorbs leakage inductance energy, clamps voltage spikes, and mitigates ringing across the main switches. It enables ZCS at the turn-off for the main semiconductors and ZCS at both turn-on and turn-off for the rectifier diodes. Compared to the design in [9], this circuit operates with fewer components, supports higher switching frequencies, and reduces prototype size. The clamping action in both the main and auxiliary circuits allows the use of semiconductors

with lower breakdown voltages, typically characterized by lower on-resistance, thereby reducing conduction losses. However, the converter proposed by [10] redirects the absorbed energy back to the input source, which is not ideal for applications such as photovoltaic converters. This redirection leads to increased input voltage oscillations, necessitating the addition of a high-capacitance capacitor at the power source's input terminals to mitigate this issue.

The present work proposes an isolated regenerative active-clamped current-fed half-bridge (IRACCFHB) converter, building on the design presented in [10] with several modifications. This auxiliary circuit aims to clamp the main switches' voltages, recover energy from the clamping capacitor to the load, and enhance the converter's efficiency without compromising galvanic isolation. The driver circuit that triggers the auxiliary switch shares the same ground as the main switches, so isolation is not required [11]. Furthermore, the main switches are turned off under ZVS. The overall circuit diagram is shown in Fig. 2.

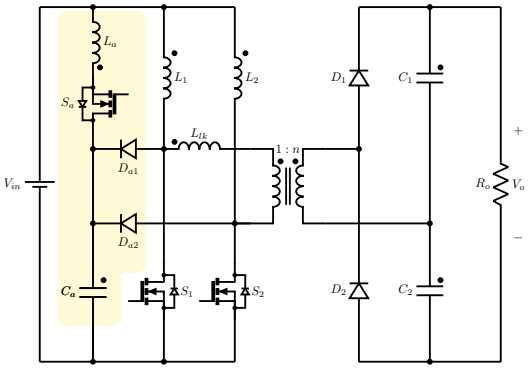

FIGURE 1. Active-clamped current-fed half-bridge (ACCFHB) converter with voltage doubler rectifier proposed by [10].

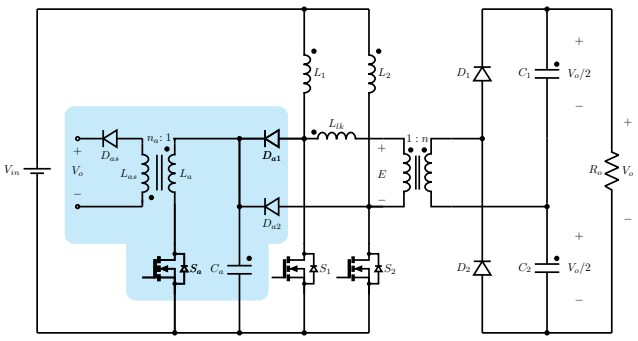

FIGURE 2. Proposed isolated regenerative active-clamped current-fed half-bridge (IRACCFHB) converter with voltage doubler rectifier.

II. ANALYSIS AND OPERATION STAGES OF THE PROPOSED CONVERTER

The proposed converter comprises a CFHB responsible for energy processing from the renewable power source to the load, and an auxiliary isolated regenerative active-clamped circuit. The auxiliary circuit clamps voltages of the main switches, avoiding voltage spikes on those, and recovers this energy, delivering it to the load. The auxiliary circuit is highlighted in Fig. 2.

The CFHB converter is composed of two boost inductors, L_1 and L_2, a high-frequency power transformer with leakage inductance L_{lk}, two main switches, S_1 and S_2, two rectifier diodes, D_1 and D_2, and two doubler voltage capacitors, C_1 and C_2. The auxiliary circuity is composed of a clamping capacitor C_a, a coupled inductor winding L_a and L_{as}, an auxiliary switch, S_a, and three auxiliary diodes, D_{a1} and D_{a2}, at the primary winding of the coupled inductor, and D_{as} at the secondary winding.

The proposed auxiliary circuit operates independently of the CFHB, except during the capacitor's charging period when one of the diodes, D_{a1} or D_{a2}, is turned on. Its operation is divided into six stages during a half-cycle of the main switching period. Before starting these stages, both main switches turn-on and conduct boost inductor currents. Diodes D_1 and D_2 are blocked, and the power transformer is not delivering energy. The doubler voltage capacitors C_1 and C_2 feed the load R_o. The auxiliary circuit is off, with no currents in either coupled inductor winding, whereas clamping capacitor, C_a, maintains a minimum voltage level ($V_{C_{amin}}$) applied over it.

Stage 1 (t_0, t_1): At t_0, the main circuit switch S_1 is turned off under zero-voltage switching (ZVS) conditions, initiating the first stage. The complete circuit is shown in Fig. 3. When S_1 is turned off, the auxiliary diode D_{a1} begins conducting when the voltage across the main switch exceeds minimum voltage level ($V_{C_{amin}}$). The rate of voltage variation across the main switch, $\frac{\mathrm{d}v}{\mathrm{d}t}$, is constrained by the clamping capacitor C_a. During this stage, a resonance occurs between C_a and L_{lk}, with the equivalent resonant circuit shown in Fig.4. The voltage over capacitor C_a increases until it reaches its maximum value ($V_{C_{amax}}$). Simultaneously, current begins to flow through the leakage inductance of the high-frequency transformer, $i_{L_{lk}}$, starting from zero and ending at $I_{L_{1max}}$, the same value as the boost inductor L_1. The main waveforms for a half-cycle of the main switching period can be seen in Fig. 5.

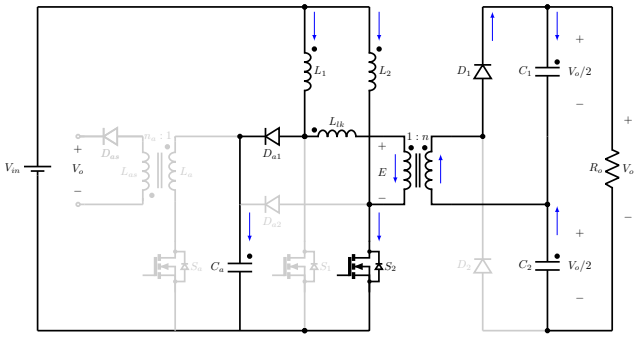

FIGURE 3. Circuit for stage 1.

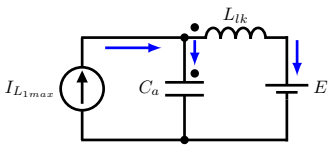

FIGURE 4. Equivalent resonant circuit for stage 1.

Throughout this stage, the voltage across switch S_1 is equal to that across C_a. When the current in L_{lk} reaches $I_{L_{1max}}$, the current in the auxiliary diode D_{a1} reaches zero, decoupling the auxiliary circuit from the main circuit and ending stage 1. The voltage across S_1 is clamped to the output voltage referred to the primary side of the high-frequency transformer, given by $E = V_o/(2n)$, where n is the turns ratio of the high-frequency transformer.

The voltage across C_a and the current through L_{lk} during stage 1 are described by (1) and (2), respectively. The time duration of this stage is calculated using (3), where the angular frequency for this equivalent circuit is denoted as ω_1, and the characteristic impedance as Z_1.

$$v_{C_a}(t) = E + V_{Emin}cos(\omega_1 t) + I_{L_{1max}} Z_1 sin(\omega_1 t) \quad (1)$$

$$i_{L_{lk}}(t) = I_{L_{1max}}[1 - cos(\omega_1 t)] + \left(\frac{V_{Emin}}{Z_1}\right) sin(\omega_1 t) \quad (2)$$

$$\Delta t_1 = \frac{1}{\omega_1}\left[arcsin\left(\frac{V_{Emax}}{V_1}\right) - arcsin\left(\frac{V_{Emin}}{V_1}\right)\right] \quad (3)$$

The equations presented in 4, 5 and 6 are voltages defined to simplify the equations above.

$$V_{Emin} = V_{C_{amin}} - E \quad (4)$$

$$V_{Emax} = V_{C_{amax}} - E \quad (5)$$

$$V_1 = \sqrt{V_{Emin}^2 + (I_{L_{1max}} Z_1)^2} \quad (6)$$

Stage 2 (t_1, t_2): The complete circuit for this stage is shown in Fig.6. During this stage, the main switch S_1 is turned off, maintaining the clamping capacitor C_a voltage at E. No current flows through the coupling inductor windings L_a and L_{as}. The auxiliary circuit is decoupled from the main circuit. The current in L_{lk} decreases linearly, matching the decline of the boost inductor L_1, until it reaches $I_{L_{1min}}$ by the stage's conclusion. The behavior of the leakage inductance of the high-frequency transformer current also follows a linear decrease, as defined by (7). The time duration of this stage is calculated using (8), where the main switches duty cycle and switching period are denoted as D and T, respectively.

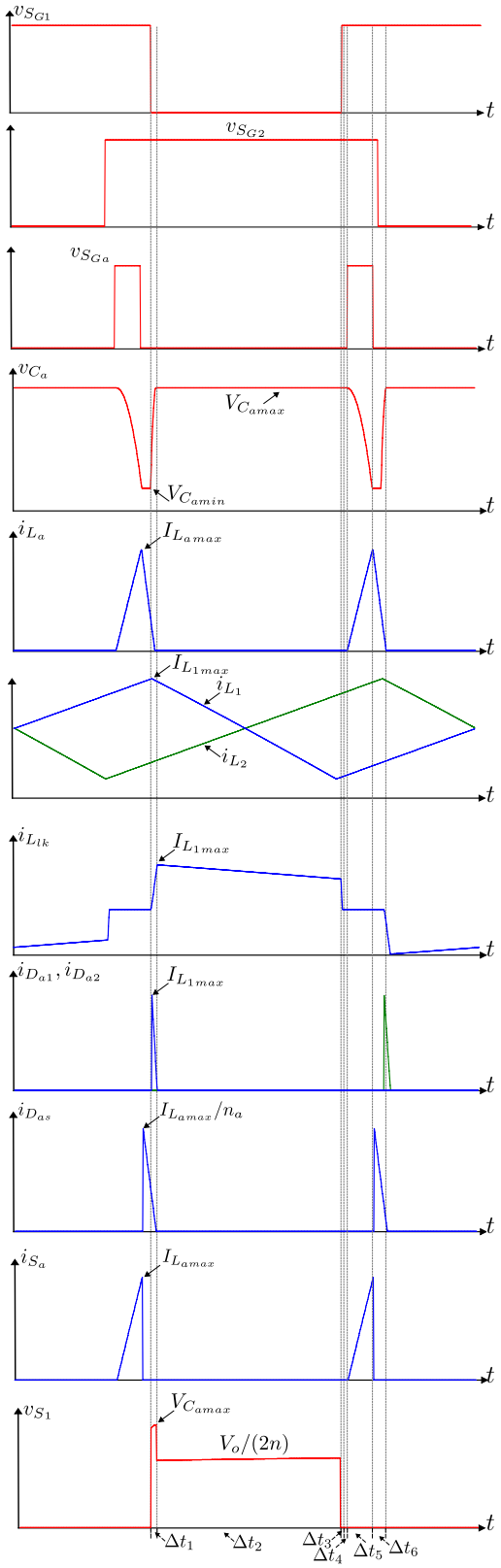

FIGURE 5. Waveforms of a half commutation period of the proposed IRACCFHB.

$$i_{L_{lk}}(t) = I_{L_{1max}} - \left(\frac{E - V_{in}}{L_1 + L_{lk}}\right)t \tag{7}$$

$$\Delta t_2 = (1 - D)T - \Delta t_1 \tag{8}$$

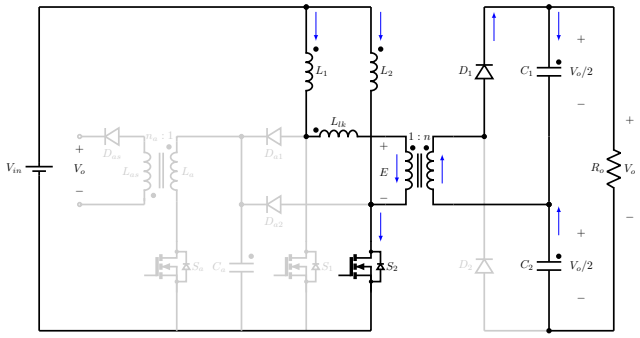

FIGURE 6. Circuit for stage 2.

Stage 3 (t_2, t_3): begins when the main switch S_1 is turned on. The circuit configuration for this stage is illustrated in Fig. 7. Upon activation of S_1, current begins to flow from L_1 through S_1, causing an increase in L_1's current. Simultaneously, all energy stored in the leakage inductance L_{lk} is discharged through diode D_1 into the load and capacitor C_1 of the voltage doubler rectifier. By the end of this stage, the current in L_{lk} diminishes to zero. The voltage across L_{lk} equals the negative output voltage relative to the primary side of the high-frequency transformer, maintaining a constant value. Specifically, this voltage remains $-E$ during this entire stage. The voltages and currents within the auxiliary circuit remain unchanged throughout Stage 3. The time duration of this stage is calculated using (9), where $I_{L_{1min}}$ is the minimum value in leakage inductance L_{lk} before its totally discharging.

$$\Delta t_3 = \frac{I_{L_{1min}} L_{lk}}{E} \tag{9}$$

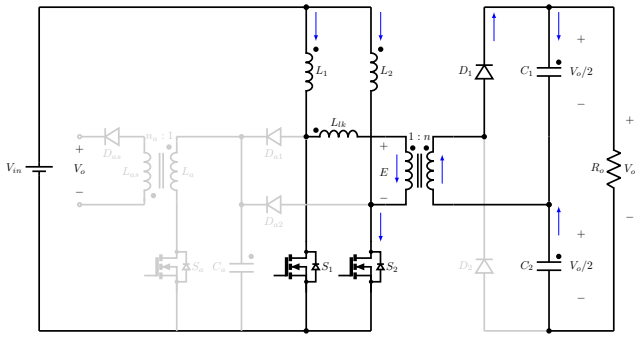

FIGURE 7. Circuit for stage 3.

Stage 4 (t_3, t_4): begins when the current through diode D_1 reaches zero at t_3. The complete circuit configuration for this stage is depicted in Fig.8. During Stage 4, capacitors C_1 and C_2 of the voltage doubler rectifier supply power to the load. The currents flowing through main switches S_1 and S_2 correspond to the currents in their respective boost inductors. Throughout this stage, the voltages and currents in the auxiliary circuit remain constant. The Δt_4 is determined according to (10), where Δt_5 and Δt_6 represent the durations of stages 5 and 6, respectively.

$$\Delta t_4 = \frac{T}{2} - \Delta t_2 - \Delta t_3 - \Delta t_5 - \Delta t_6 \tag{10}$$

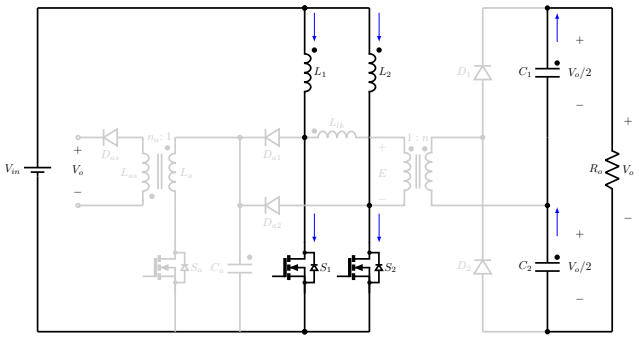

FIGURE 8. Circuit for stage 4.

Stage 5 (t_4, t_5): begins at t_4 when the auxiliary switch S_a turns on. The complete circuit configuration for Stage 5 is illustrated in Fig.9. During this stage, main switches S_1 and S_2 are turned on, whereas the auxiliary circuit operates independently from the main circuit. When S_a is activated under ZCS conditions, a resonance occurs between capacitor C_a and the primary winding L_a of the coupling inductor. Figure 10 depicts the resonant circuit behavior during this stage. By the end of Stage 5, the voltage across C_a reaches its minimum level, denoted as $V_{C_{amin}}$, whereas the current through L_a reaches its maximum value, $I_{L_{amax}}$. The voltage over the C_a and current through L_a in stage 5 are determined by (11) and (12), respectively, where ω_5 is the resonant frequency between L_a and C_a, defined in (13), Z_5 is the resonant impedance, defined by (14), D_a is the duty cycle of the auxiliary switch, and f_{sa} is the switching frequency of the auxiliary switch. The time duration of this stage is calculated using (15).

$$v_{C_a}(t) = V_{C_{amax}} cos(\omega_5 t) \tag{11}$$

$$i_{L_a}(t) = \frac{V_{C_{amax}}}{Z_5} sin(\omega_5 t) \tag{12}$$

$$\omega_5 = \frac{1}{\sqrt{L_a C_a}} \tag{13}$$

$$Z_5 = \sqrt{\frac{L_a}{C_a}} \tag{14}$$

$$\Delta t_5 = \frac{D_a}{f_{sa}} \tag{15}$$

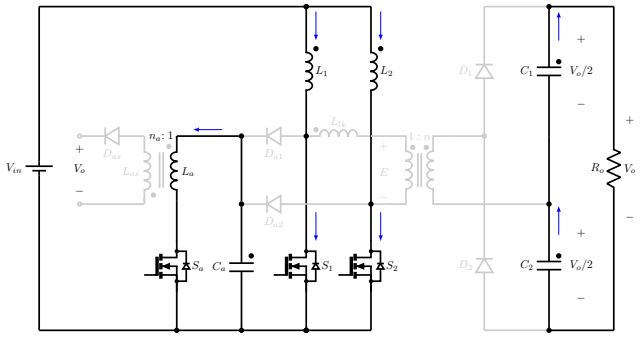

FIGURE 9. Circuit for stage 5.

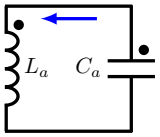

FIGURE 10. Equivalente resonant circuit for stage 5.

Stage 6 (t_5, t_6): involves the complete discharge of the energy stored in the coupled inductor of the auxiliary circuit. The circuit configuration for this stage is depicted in Fig.11. It starts when the auxiliary switch S_a is turned off under hard switching, at the moment the current flowing through it reaches its peak value $I_{L_{amax}}$, which is the same current flowing through the primary winding L_a. Due to the coupling ratio n_a, this value referred to the secondary side is $I_{L_{asmax}} = I_{L_{amax}}/n_a$. This energy is discharged to the load through the auxiliary diode D_{as}. When the current in L_a decreases to zero, and D_{as} is blocked. The process of discharging energy from L_{as} to the load is represented by the circuit in Fig. 12. The instantaneous current in L_{as} is governed by (16), and the duration of Stage 6 is calculated using (17).

$$i_{L_{as}}(t) = I_{L_{asmax}} - \frac{V_o t}{L_{as}} \tag{16}$$

$$\Delta t_6 = \frac{I_{L_{asmax}} L_{as}}{V_o} \tag{17}$$

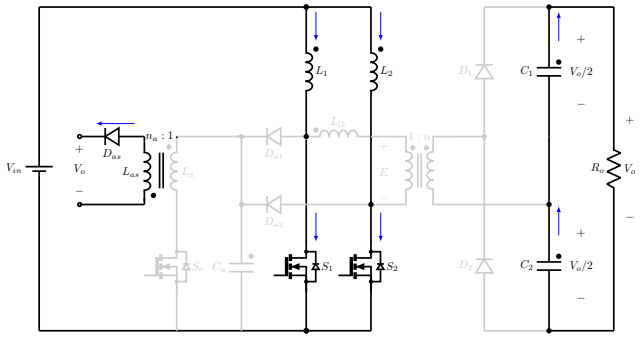

FIGURE 11. Circuit for stage 6.

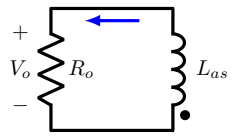

FIGURE 12. Equivalent discharging circuit for stage 6.

The static gain M of the converter expresses the relationship between the output voltage and the input voltage based on steady-state operation parameters. This gain is determined using the volt-second balance principle applied to either boost inductor L_1 or L_2, assuming the average voltage across these inductors over a switching cycle is zero.

As depicted in Fig. 13, the impact of the auxiliary circuit on the voltage ratio is minimal, indicating its role primarily as a clamp and regenerative circuit for energy transfer from the clamping capacitor to the load.

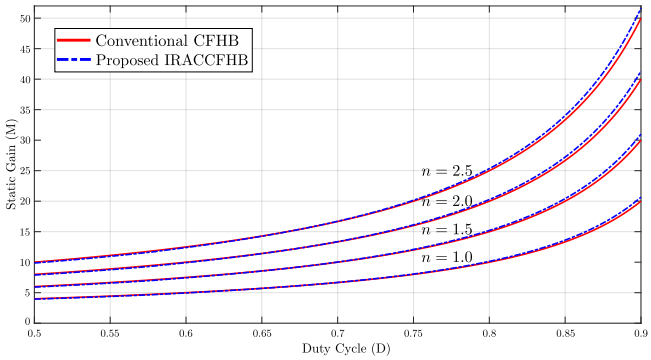

FIGURE 13. Variation of the voltage ratio (M) concerning the variation of the main switches' duty cycle (D) for some values of n.

III. DESIGN CONSIDERATIONS FOR THE PROPOSED CONVERTER

A. Project of Components

The main circuit of the proposed converter is designed to transfer power from a power source to a load whereas maintaining galvanic isolation. It incorporates a voltage doubler circuit with two capacitors and two diodes. The duty cycle D is determined by the converter's input and output voltages and the transformer's turns ratio, as expressed in (18).

$$D = 1 - 2n\frac{V_{in}}{V_o} \tag{18}$$

Since it operates as a current-fed converter, the input current is shared between two boost inductors. The values of these boost inductors, L_1 and L_2, and the doubler voltage capacitors, C_1 and C_2, can be calculated using (19) and (20), respectively, where f_s is the main switching frequency, ΔI_L is the ripple of the boost inductor current, and ΔV_o is the ripple of output voltage.

$$L_1 = L_2 = \frac{V_{in} D}{\Delta I_L f_s} \tag{19}$$

$$C_1 = C_2 = \frac{P_o D}{2V_o \Delta V_o f_s} \tag{20}$$

To ensure that the activation of the auxiliary switch is synchronized with the activation of the main switches, turning on and off whereas main switches are turned on, duty cycle of auxiliary switch must be defined respecting (21), whereas (22) is utilized to calculate the timing offset to active auxiliary switch centralized relative to main switches' activation, where T_{sa} represents the switching period of the auxiliary switch S_a.

$$D_a \leq 2(D - 0.5) \tag{21}$$

$$T_{sashift} = \frac{1 - D_a}{2} T_{sa} \tag{22}$$

The design of the auxiliary circuit elements begins with establishing the maximum voltage across the main switches, corresponding to the maximum voltage across the clamping capacitor ($V_{C_{amax}}$). This value must be carefully determined to ensure it does exceed but should not be much higher than the voltage across the primary winding of the high-frequency transformer, thereby maintaining the main switches' voltage below their breakdown level. Simultaneously, the minimum voltage across the clamping capacitor at the end of the energy discharge period ($V_{C_{amin}}$) is set as a percentage of $V_{C_{amax}}$. $V_{C_{amin}}$ should also be higher than the voltage across the primary winding of the high-frequency transformer. The relationship between $V_{C_{amax}}$ and $V_{C_{amin}}$ is defined by (23), where the coefficient k_1, which scales $V_{C_{amin}}$ relative to $V_{C_{amax}}$, should be less than 1.

$$V_{C_{amin}} = k_1 V_{C_{amax}} \tag{23}$$

The value of capacitor C_a is determined by (24), derived from manipulating (1), (2), and (12). Upon examination of this equation, it becomes evident that the clamping capacitance is directly proportional to the leakage inductance value of the high-frequency transformer, L_{lk}. This implies that as the energy dissipation in the high-frequency transformer increases, the capacitance must be correspondingly increased to withstand overvoltage conditions. Furthermore, the capacitance of C_a is proportional to the square of the maximum current in the boost inductor L_1. Therefore, larger capacitance values are required when L_1 carries higher currents, ensuring proper voltage clamping and protection of the main switches and other components.

$$C_a = \frac{L_{lk} I_{L_{1max}}^2}{V_{C_{amax}}(1 - k_1)[V_{C_{amax}}(1 + k_1) - 2E]} \tag{24}$$

Another crucial parameter to define is the amount of power that the auxiliary circuit will recover from the clamping capacitor C_a and deliver to the load, denoted as P_{aavg}. This value is determined based on the energy recovered when the main switches turn-off, which is subsequently transferred by the auxiliary circuit to ensure high converter efficiency. P_{aavg} is specifically defined as the average power of the auxiliary circuit flowing from the clamping capacitor C_a to the coupled inductor L_a during Stage 5. It is calculated using (25). This parameter quantifies the effective power transfer capability of the auxiliary circuit in maintaining overall converter performance.

$$P_{aavg} = \frac{1}{T_{sa}} \int_{t_4}^{t_5} v_{C_a} i_{C_a} dt = \frac{C_a V_{C_{amax}}^2 sin^2(\omega_5 \Delta t_5)}{2T_{sa}} \tag{25}$$

Thus, to calculate the value of L_a, the terms of (25) should be rearranged, resulting in (26).

$$L_a = \frac{\Delta t_5^2}{C_a \left\{ arcsin\left[\sqrt{\frac{2P_{aavg} T_{sa}}{C_a V_{C_{amax}}^2}} \right] \right\}^2} \tag{26}$$

Indeed, as indicated in (26), the design of the primary inductance L_a is influenced significantly by the capacitance of C_a and the maximum voltage specified for the clamping capacitor. Additionally, it's evident that the duration Δt_5, during which the auxiliary switch S_a remains on, directly impacts the power recovered by the auxiliary circuit. A longer Δt_5 results in greater energy transfer and, thus, higher power delivered to the load through Stage 5 of operation. However, increasing power transfer through the auxiliary circuit also introduces trade-offs. Higher power levels lead to increased conduction losses in the auxiliary switch and losses in the magnetic core of the coupled inductor. These losses can affect overall efficiency and thermal management within the converter system. Therefore, in designing L_a and determining Δt_5, careful consideration is required to balance these factors and optimize the converter's performance and reliability.

The determination of the secondary inductance L_{as} of the coupled inductor is governed by (27), where n_a represents the turn ratio defined by the designer. It's crucial to note that n_a should not be excessively high, as this would increase voltage across the auxiliary diode D_{as}.

$$L_{as} = n_a^2 L_a \tag{27}$$

B. Determination of Components

This subsection aims to present the procedure for determining the components of the proposed converter. Table 1 shows the input parameters of the designed converter.

The CFHB project starts by determining the duty cycle of the main switches. To achieve the desired output voltage, it is essential to define the power transformer turns ratio such that $D > 0.5$. Consequently, the turns ratio was set to $n = 2.25$. Using this value and equation (18), the duty cycle D was calculated to be 0.575.

The next step was calculating boost inductance, doubler voltage capacitance, and $I_{L_{1max}}$. Defining a boost current ripple ΔI_L equal to 20 % of current input, using (19),

TABLE 1. Input Parameters of Proposed Converter

Parameters	Values
V_{in}	37.8 V
P_{in}	350 W
V_o	400 V
f_s	100 kHz
f_{sa}	200 kHz
R_o	482 Ω
$L_1 = L_2$	131 μH
$C_1 = C_2$	470 nF
C_a	100 nF
Power transformer	$L_{lk} = 2.25$ μH $n = 2.25$ Prim: 12 turns 10 Wires # 27 AWG Sec: 27 turns 4 Wires # 27 AWG Core: EE 42/21/15 Thornton
Coupled inductor	$L_a = 42$ μH $L_{as} = 46$ μH $n_a = 1.05$ Prim: 11 turns 3 Wires #33 AWG Sec: 11 turns 3 Wires #33 AWG Core: EE 20/10/5 Thornton

$L_1 = L_2 = 123.5$ μH. Defining ΔV_o of 1 % of output voltage, using (20), $C_1 = C_2 = 477.76$ nF. Ending this step, $I_{L_{1max}} = 5.28$ A.

With D determined, according to (21), the auxiliary switch duty cycle must be lower than 0.1495. It was defined as $D_a = 0.10$ to ensure this switch will turn-on and off whereas the main switches are turned on, and the delay time to activate auxiliary switch is $T_{sashift} = 2.25$ μs. $V_{C_{amax}}$ was defined as 140 V and $k_1 = 0.95$, to ensure both maximum and minimum voltages over clamping capacitor are higher than output voltage at primary side of high-frequency transformer. Therefore, $V_{C_{amin}}$ is equal to 133 V. Determined voltages and currents in the auxiliary circuit, C_a is calculated using (24) as 94.02 nF. P_{aavg} must be defined as low percentage value regarding to input power P_{in}, which it corresponds to tuning-off main switches losses recovered by auxiliary circuit. So, defining $P_{aavg} = 3$ % of P_{in}, $P_{aavg} = 10.5$ W. With those values, by (26), L_a is calculated as $L_a = 45.77$ μH. Defining $n_a = 1.0$, $L_{as} = 45.77$ μH

IV. RESULTS

To validate the performance of the proposed converter for microinverter application, a 350 W prototype was built, presented in Fig. 14. Instead of a photovoltaic solar panel it was used a power source. The load consisted of a 482 Ω (350 W) resistor.

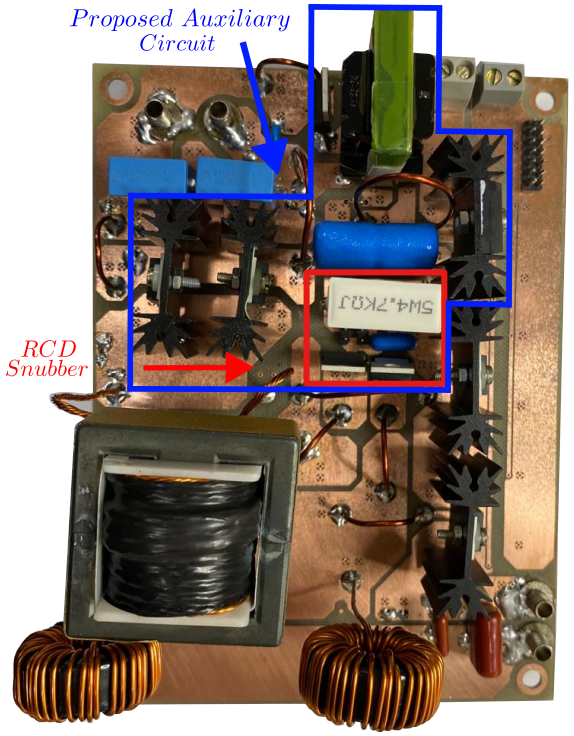

FIGURE 14. Experimental prototype (159mm x 121mm).

For constructing this prototype, low breakdown voltage MOSFETs were selected for the main switches. Among the models available in the laboratory, the IPP110N20N3 from Infineon Technologies was chosen due to its low $R_{DS,on}$ of 10.7 mΩ, making it suitable for high-frequency operation. As the auxiliary switch S_a needs to withstand relatively high voltage, the C2M0080120A SiC MOSFET from Wolfspeed Inc. was chosen for its lower conduction resistance and output capacitance compared to similar models. For the rectifier diodes D_1 and D_2, as well as the auxiliary diodes D_{a1}, D_{a2}, and D_{as}, the C3D12065 model from Wolfspeed Inc. was selected due to its ultra-low reverse recovery time and charge. The gate driver chosen for switching the converter's switches was the UCC5390 model from Texas Instruments, due to its isolation feature and wide input and output voltage range.

The inductance value achieved for the implemented boost inductances was 131 μH. The waveforms of the currents in boost inductors L_1 and L_2 are shown in Fig. 15, where it is possible to see the delay time of the switching cycle between the commands of the main switches. $I_{L_{1avg}}$ is the average current that flows through boost inductor L_1, equal to $I_{L_{2avg}}$. This value is calculated as 4.399 A, with an ΔI_L of 20 % of I_{in}, reaching a maximum value of $I_{L_{1max}} = I_{L_{2max}} = 5.278$ A. Therefore, with the implemented inductance value, the current values were $I_{L_{1avg}} = I_{L_{2avg}} = 4.675$ A and $I_{L_{1max}} = I_{L_{2max}}$ and 5.875 A. Besides that, with input voltage equal to $V_{in} = 37.83$ V, output voltage was reached as $V_{in} = 400.37$ V.

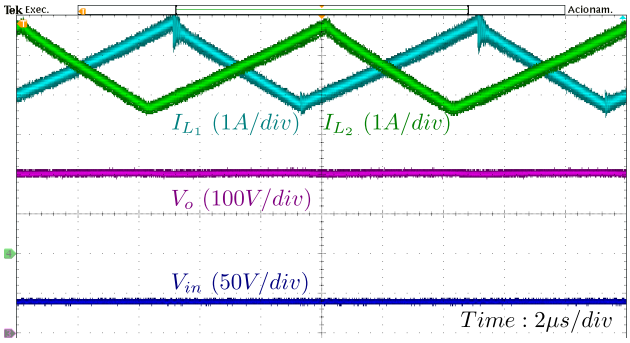

FIGURE 15. Currents through the boost inductors L_1 and L_2, input voltage V_{in} and output voltage V_o.

Figure 16 displays the voltage waveforms across the clamp capacitor C_a and the main switch S_1, with similar results obtained for the main switch S_2. The graph shows that the voltage on the main switch increases from $V_{C_{amin}}$ to $V_{C_{amax}}$ whereas the auxiliary diode D_{a1} conducts current. When D_{a1} stops conducting, the voltage on S_1 is theoretically limited to $V_o/(2n)$, and C_a reaches $V_{C_{amax}}$. However, as observed, after D_{a1} ceases current flow, the voltage on S_1 is clamped slightly above $V_o/(2n)$ due to the magnetizing inductance and series resistance in the high-frequency transformer. In bench tests, the maximum and minimum voltages across the capacitor were $V_{C_{amax}} = 146.73$ V and $V_{C_{amin}} = 138.07$ V, respectively. The design values for these voltages are $V_{C_{amax}} = 140$ V and $V_{C_{amin}} = 133$ V. The coefficient obtained in bench tests was $k_1 = 0.941$. The actual values for clamping voltages and coefficients were slightly different from the calculated ones due to the intrinsic capacitances and inductances in the construction of the mosfets in parallel with the capacitor.

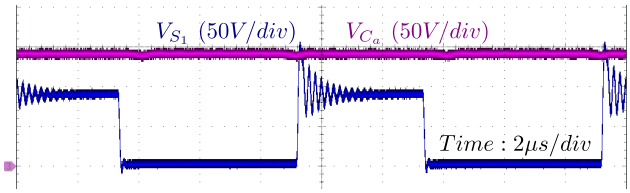

FIGURE 16. Voltages across the clamping capacitor C_a and the main switch S_1.

Figure 17 shows the voltage and current waveforms for the main switch S_1. The peak voltage reached $V_{S_{1max}} = 151.23$ V, whereas the maximum current in S_1 was $I_{S_{1max}} = 9.53$ A. The maximum voltage on the main switch is $V_{S_{1max}} = 140$ V. As previously mentioned, the increase in the maximum voltage on the main switch S_1, as well as for S_2, is due to the intrinsic capacitances and inductances of these semiconductors. Additionally, it is observed that ZVS occurs when S_1 is turned off, as highlighted in Fig. 18. According to [12], this type of commutation is classified as pseudo-ZVS, since the current waveform of S_1 rapidly drops to zero, causing a very small overlapping with the voltage waveform of S_1 at the moment it begins to rise.

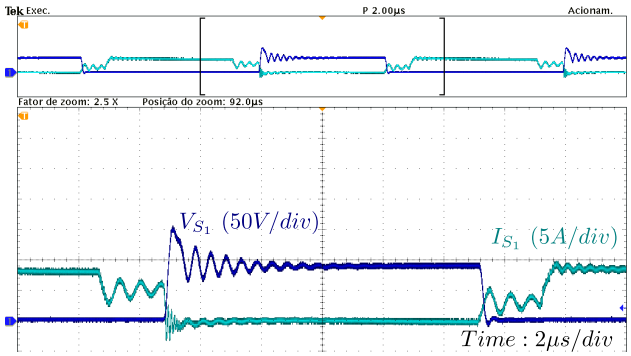

FIGURE 17. Voltage and current across the main switch S_1.

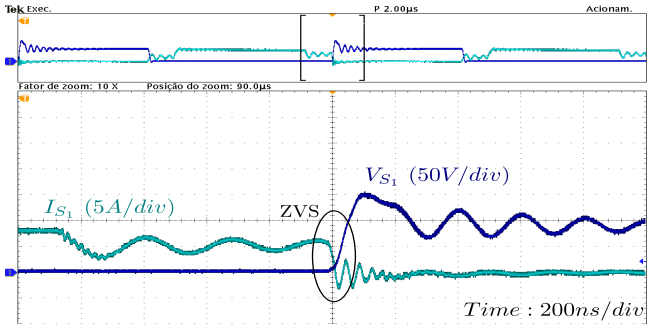

FIGURE 18. ZVS during the turn-off of the main switch S_1 due to the presence of the auxiliary circuit.

Figure 19 shows the voltage and current waveforms for the auxiliary switch S_a obtained from bench tests. The peak voltage reached $V_{S_{amax}} = 601.97$ V, whereas the maximum current in S_a was $I_{S_{amax}} = 1.47$ A. The peak current of the auxiliary switch is nearly equal to the calculated value. However, the maximum voltage observed across the auxiliary switch S_a was significantly higher (20 % more than the calculated value). This occurred because the output capacitance of the chosen mosfet for the auxiliary switch is relatively high. Nevertheless, this semiconductor can withstand voltage peaks up to 1200 V. Additionally, it is observed that ZCS occurs when S_a is turned on, as highlighted in Fig. 20.

Figure 21 depicts the voltage waveform across the clamp capacitor C_a and the currents in the primary and secondary windings of the coupled inductor L_a after implementing the proposed converter. In the primary winding of the coupled inductor L_a, which is in series with the auxiliary switch S_a, the maximum current value is $I_{L_{amax}} = 1.47$ A for the implemented converter, compared to the designed value of $I_{L_{amax}} = 1.45$ A. In the secondary winding, during the process of discharging the stored energy to the load, the maximum current value in the secondary winding of the coupled inductor is $I_{L_{asmax}} = 1.17$ A, reflecting the transformation ratio of the coupled inductor being $n_a = 1.05$ instead of the designed unity ratio.

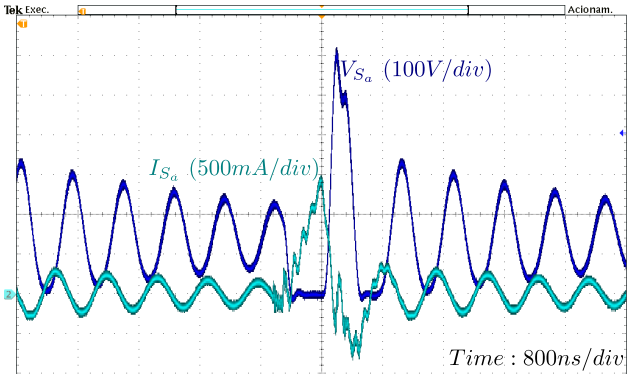

FIGURE 19. Voltage and current across the auxiliary switch S_a.

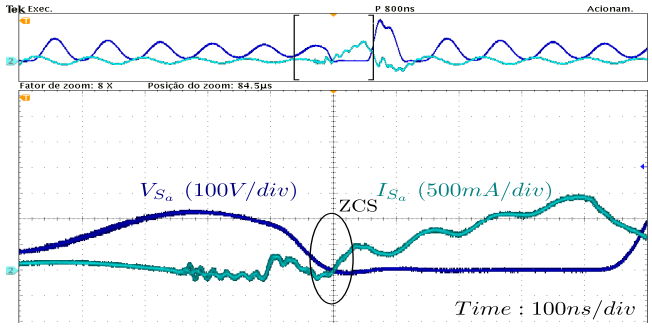

FIGURE 20. ZCS during the turn-on of the auxiliary switch S_a.

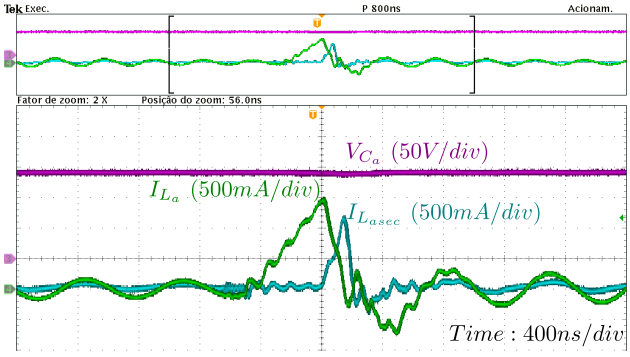

FIGURE 21. Voltage across the clamp capacitor C_a, and currents in the primary and secondary windings of the coupled inductor.

The proposed IRACCFHB was tested across an input voltage range from 35.8 V to 39.8 V to evaluate its performance at different operating points. Figure 22 shows the measured efficiency of the proposed converter under various load conditions, obtained using the Tektronix PA4000 high-performance power analyzer. The proposed converter achieved an efficiency of 94.74 % at full load. A peak efficiency of 94.88 % was observed at an input voltage of 37.8 V, while the minimum efficiency recorded was 88.49 % at an input voltage of 35.8 V.

To evaluate the performance of the clamping circuit, the proposed solution was compared to the RCD snubber circuit, which is simpler and cheaper to implement and was adapted

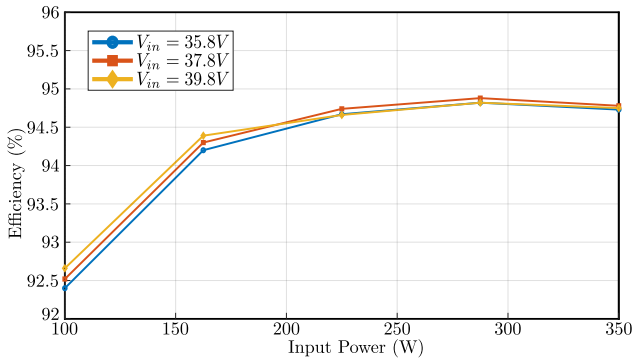

FIGURE 22. The measured efficiency of the proposed IRACCFHB under various load conditions and input voltage levels.

from [13]. This clamping circuit was integrated into the same printed circuit board (PCB), where it can be seen at Fig. 14, for each of the main switches and was used with the active clamping function disabled. The snubber resistor used was $R_s = 1.56$ kΩ, while the snubber capacitor was $C_s = 56$ nF. The diodes employed were the same as those used for D_{a1} and D_{a2} in the active auxiliary circuit.

Tests using the RCD circuit were conducted for various load values, always with the nominal input voltage. The highest efficiency achieved was 91.61%. Figure 23 presents a comparison of the efficiency curves for the proposed and passive solutions at an input voltage of $V_{in} = 37.8$ V.

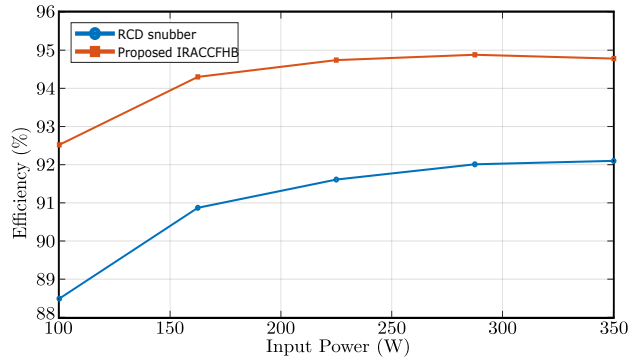

FIGURE 23. Comparasion of efficiency's curves of the proposed IRACCFHB and RCD snubber with for various load conditions at $V_{in} = 37.8\ V$ and $V_o = 400\ V$.

V. CONCLUSION

In this paper, an isolated auxiliary circuit for the CFHB converter to clamp the main switch voltage, preventing high voltage spikes on the main switches and recovering energy from the clamping capacitor to the load through coupled inductor windings and an auxiliary diode. This circuit achieves ZVS at turn-off for the main switches and ZCS at turn-on for the auxiliary switch. The clamping action enables the use of semiconductors with lower breakdown voltage for the CFHB, generally resulting in lower losses and increased converter efficiency.

Compared to other clamping circuits for the CFHB in the literature, the proposed auxiliary circuit uses only one active switch, does not require a series inductor with the transformer, and the driver circuit for the auxiliary switch does not need to be isolated, as it shares the same source with the main switches. Moreover, the energy recovered by the auxiliary circuit is delivered to the load, achieving 94.88% of efficiency operating at full load. Also, in the same PCB of the proposed converter, connections for RCD snubbers was included to perform a comparative analysis. Compared to the CFHB with RCD snubber the proposed converter obtained an efficiency increase of 3.27% at full load and nominal conditions of input and output voltages.

ACKNOWLEDGMENT

The present work was carried out with the support of the Coordenação de Aperfeiçoamento de Pessoal de Nível Superior - Brazil (CAPES) - Financing Code 001, CNPq processes 405700/2021-0 and 306633/2022-1, NAPI Sudoeste, Fundação Araucária and UTFPR - Campus Pato Branco.

AUTHOR'S CONTRIBUTIONS

G. E. R SILVA: Conceptualization, Data Curation, Formal Analysis, Investigation, Methodology, Resources, Software, Validation, Visualization, Writing – Original Draft, Writing – Review & Editing. **C. M. O. STEIN**: Conceptualization, Data Curation, Formal Analysis, Funding Acquisition, Investigation, Methodology, Project Administration, Software, Supervision, Validation, Visualization, Writing – Review & Editing. **J. P. COSTA**: Funding Acquisition, Project Administration, Writing – Review & Editing. **E. G. CARATI**: Funding Acquisition, Project Administration, Writing – Review & Editing. **R. CARDOSO**: Funding Acquisition, Project Administration, Writing – Review & Editing. **G. W. DENARDIN**: Funding Acquisition, Project Administration, Writing – Review & Editing. **J. B. B. QUISPE**: Software, Validation, Writing – Review & Editing.

PLAGIARISM POLICY

This article was submitted to the similarity system provided by Crossref and powered by iThenticate – Similarity Check.

REFERENCES

[1] A. M. S. S. Andrade, L. Schuch, M. L. da Silva Martins, "Analysis and design of high-efficiency hybrid high step-up dc–dc converter for distributed pv generation systems", *IEEE Transactions on Industrial Electronics*, vol. 66, no. 6, pp. 3860 – 3868, May 2019, doi:10.1109/TIE.2018.2840496.

[2] H. Kim, C. Yoon, S. Choi, "An improved current-fed zvs isolated boost converter for fuel cell applications", *IEEE Transactions on Power Electronics*, vol. 25, no. 9, pp. 2357 – 2364, September 2010, doi:10.1109/TPEL.2010.2048044.

[3] S. A. Teston, E. G. Carati, R. Cardoso, J. P. da Costa, C. M. de O. Stein, "Efeito da Conexão do Capacitor de Grampeamento Sobre a Corrente de Entrada no Conversor Alimentado em Corrente Meia-Ponte ZVS com Grampeamento Ativo", *Eletrônica de Potência*, vol. 21, no. 3, pp. 179–189, Sept. 2016, doi:10.18618/REP.2016.3.2587.

[4] R. Kanthimathi, J. Kamala, "Analysis of different Flyback Converter Topologies", *2015 International Conference on Industrial Instrumentation and Control (ICIC)*, pp. 1248–1252, July 2015, doi:10.1109/IIC.2015.7150939.

[5] S. A. Teston, E. G. Carati, J. P. da Costa, R. Cardoso, C. M. D. O. Stein, "Comparison of two connection possibilities of the clamp capacitor in the active-clamped zvs current-fed half-bridge converter", *2015 IEEE 13th Brazilian Power Electronics Conference and 1st Southern Power Electronics Conference (COBEP/SPEC)*, pp. 1–6, February 2016, doi:10.1109/COBEP.2015.7420028.

[6] S.-K. Han, H.-K. Yoon, G.-W. Moon, M.-J. Youn, Y.-H. Kim, K.-H. Lee, "A new active clamping zero-voltage switching pwm current-fed half-bridge converter", *IEEE Transactions on Power Electronics*, vol. 20, no. 6, pp. 1271 – 1279, November 2005, doi:10.1109/TPEL.2005.857525.

[7] A. Rathore, A. Bhat, R. Oruganti, "Analysis and design of active clamped zvs current-fed dc-dc converter for fuel-cell to utility interface application", International Conference on Industrial and Information Systems", *International Conference on Industrial and Information Systems*, pp. 503 – 508, August 2007, doi:10.1109/ICIINFS.2007.4579229.

[8] A. K. Rathore, A. K. S. Bhat, R. Oruganti, "Wide range zvs activeclamped l-l type current-fed dc-dc converter for fuel cells to utility interface: Analysis, design and experimental results", *2009 IEEE Energy Conversion Congress and Exposition*, pp. 1153–1160, September 2009, doi:10.1109/ECCE.2009.5316540.

[9] S.-J. Jang, C.-Y. Won, B.-K. Lee, J. Hur, "Fuel cell generation system with a new active clamping current-fed half-bridge converter", *IEEE Transactions on Energy Conversion*, vol. 22, no. 2, pp. 332 – 340, May 2007, doi:10.1109/TEC.2006.874208.

[10] C. F. Moraes, E. G. Carati, J. P. da Costa, R. Cardoso, C. M. de Oliveira, "Active-clamped Zero-Current Switching Current-Fed Half-Bridge Converter", *IEEE Transactions on Power Electronics*, vol. 35, no. 7, pp. 7100 – 7109, December 2019, doi:10.1109/TPEL.2019.2959447.

[11] G. E. R. D. Silva, C. M. de Oliveira Stein, J. P. D. Costa, E. G. Carati, R. Cardoso, "Active-Clamped Circuit Zero-Current Switching Current-Fed Half-Bridge Converter With Energy Recovery", *in 2023 15th IEEE International Conference on Industry Applications (INDUSCON)*, pp. 1576–1582, 2023, doi:10.1109/INDUSCON58041.2023.10374934.

[12] S. Ben-Yaakov, G. Ivensky, *Passive Lossless Snubbers for High Frequency PWM Converters*, chap. pp. 14, APEC 99 Seminar, 1999.

[13] N. Mohan, T. M. Undeland, W. P. Robbins, *Power Electronics - Converters, Applications and Design*, Wiley, New York, 1995.

BIOGRAPHIES

Glauco Ércico Rocha da Silva received the B.S. degree in electrical engineering from the Western State University of Paraná (UNIOESTE), Foz do Iguaçu, Brazil, in 2019, and the M.Sc. degree in electric engineering from the Federal University of Technology – Paraná (UTFPR), Pato Branco, Brazil, in 2024. Currently, he is pursuing the Ph.D. degree in electrical engineering at Santa Catarina State University (UDESC), Joinville, Brazil. His research interest relates to power converter topologies, soft-switching techniques, modulation techniques for static converters, and electric vehicles.

Carlos Marcelo de Oliveira Stein received the B.S., M.S., and Ph.D. degrees in electrical engineering from the Federal University of Santa Maria, Santa Maria, Brazil, in 1996, 1997, and 2003, respectively. Since 2003, he has been with the Federal University of Technology – Paraná (UTFPR), Pato Branco, Brazil, where he is currently a Full Professor. His research interests include high-frequency power converter topologies, distributed generation, power supplies, and soft-switching techniques.

Jean Patric da Costa received the B.S. degree in electrical engineering and the M.S. and Ph.D. degrees from the Federal University of Santa Maria, Santa Maria, Brazil, in 2004, 2006, and 2010, respectively. He is currently a Professor with the Department of Electrical Engineering, Federal University

of Technology – Paraná, Pato Branco, Brazil. His research interests include control of static converters, smart grids, ancillary services, and distributed generators.

Emerson Giovani Carati received the B.S. degree (1996), the M.S. degree (1999), and the Ph.D. degree (2003) in electrical engineering from the Federal University of Santa Maria, Brazil. Since 2003, he has been with the Federal University of Technology – Paraná (UTFPR), Pato Branco, Brazil, where he is a Full Professor. His research interests are related to control of electrical machine drives, distributed power generation, and static converters.

Rafael Cardoso received the B.S. degree in electrical engineering from the Federal University of Santa Maria (UFSM), Santa Maria, Brazil, in 2001, the M.Sc. degree in electronic and computer science from the Technological Institute of Aeronautics (ITA), São Paulo, Brazil, in 2003, and the Ph.D. degree in electrical engineering from UFSM in 2008. Since 2006, he has been with the Federal University of Technology – Paraná (UTFPR), Pato Branco, Brazil, where he is currently a Full Professor. His research interests include automatic control systems, power electronics, power converter control, energy storage systems, smart grids, and power quality.

Gustavo Weber Denardin received the B.S., M.Sc., and Ph.D. degrees in electrical engineering from the Federal University of Santa Maria, RS, Brazil, in 2002, 2004, and 2012, respectively. Since 2005, he has been with the Federal University of Technology – Paraná, Pato Branco, Brazil, where he is currently a Full Professor. His research interests include embedded systems, real-time operating systems, instrumentation, communication systems, wireless sensor/actuator networks, and smart grids.

Jhon Brajhan Benites Quispe received the B.S. degree in electronic engineering from the National University of Engineering (UNI), Lima, Peru, the M.Sc. and Ph.D. degree in electrical engineering from São Paulo State University Júlio de Mesquita Filho (UNESP). Currently, he is pursuing a postdoctoral degree at Santa Catarina State University. His research interests include electric mobility, microgrids, and renewable energy."